ACS APPLIED MATERIALS & INTERFACES

Research Article

Cite This: ACS Appl. Mater. Interfaces 2018, 10, 4961−4970

www.acsami.org

Convenient and Robust Route to Photoswitchable Hierarchical Liquid Crystal Polymer Stripes via Flow-Enabled Self-Assembly

Xiao Li,[†,‡] Bo Li,[†] Ming He,[†] Wei Wang,[†,§] Tianjie Wang,[‡] Aurelia Wang,[†] Jiwoo Yu,[†] Zhonglin Wang,[†] Suck Won Hong,[∥] Myunghwan Byun,[⊥] Shaoliang Lin,[*,§] Haifeng Yu,[*,‡] and Zhiqun Lin[*,†]

[†]School of Materials Science and Engineering, Georgia Institute of Technology, Atlanta, Georgia 30332, United States

[‡]Department of Material Science and Engineering, and Key Laboratory of Polymer Chemistry and Physics of Ministry of Education, Peking University, Beijing 100871, P. R. China

[§]School of Materials Science and Engineering, East China University of Science and Technology, Shanghai 200237, P. R. China

[∥]Department of Cogno-Mechatronics Engineering, Department of Optics and Mechatronics Engineering, Pusan National University, Busan 46241, Republic of Korea

[⊥]Department of Advanced Materials Engineering, Keimyung University, Daegu 704-701, Republic of Korea

Supporting Information

ABSTRACT: Hierarchically arranged stripes of photoswitchable liquid crystal polymers (LCPs) containing azobenzene moieties were conveniently crafted via a flow-enabled self-assembly (FESA). Interestingly, by subjecting a drop of LCP solution to dry in a restricted geometry comprising two nearly parallel plates with a stationary upper plate and a movable lower plate that programmably traveled in a "stop-and-move" manner during the FESA process, photoswitchable LCP stripes were yielded, displaying two modes of deposition, namely, periodic primary stripes of large dimensions and regularly spaced secondary stripes of small dimensions situated between adjacent primary stripes (i.e., forming hierarchical LCP stripes). Notably, these hierarchical azobenzene moieties-containing stripes demonstrated sequential photoinduced reversible phase transition (i.e., photoswitching) due to the thickness difference between primary and secondary stripes. A UV light-induced expansion effect was observed on the LCP stripes. Clearly, such rapid creation of hierarchical stripes by FESA represents a robust means of organizing polymers, nanoparticles, colloids, DNA, etc. into complex yet ordered patterns over a large area in a simple and controllable manner for potential use in surface relief grating, photoactuators, photoswitchable devices, antifake labels, etc.

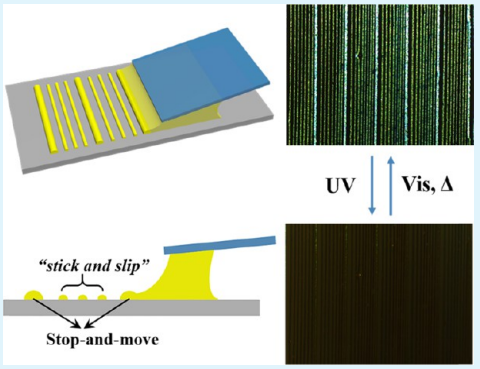

KEYWORDS: *flow-enabled self-assembly, hierarchical structure, azo-containing liquid crystalline polymer, photoinduced phase transition, photoexpansion effect*

INTRODUCTION

Azobenzene has been widely recognized as an appealing molecular switch for light-driven devices owing to the large yet reversible changes in its dipole moment and molecular shape that occur upon photoisomerization.[1] Recently, several intriguing studies have centered on azo-containing LCPs, such as voxelated liquid crystalline elastomers,[2] photoactuated microfluidics system,[3] and photoinduced wave propagation.[4] Azobenzene moieties typically exist in a more stable trans-conformation as a rodlike molecule. The irradiation of azobenzene-containing molecule with UV light (365 nm) produces a large fraction of the bent cis- isomer, which reverts to the trans- state either thermally or upon exposure to visible light.[5−7] For liquid crystal polymers (LCPs) containing azobenzene moieties, the rodlike trans- azo mesogens stabilize the liquid crystalline (LC) state, whereas the bent cis- azo units often destabilize the LC state. Such molecular-level rodlike-to-bent photoisomerization (and vice versa) and the associated photoinduced microscopic phase transition process (e.g., nematic LC-to-isotropic transition and vice versa) render azobenzene-containing LCPs for use in two-dimensional data storage and optical switch,[8,9] surface-relief grating,[10,11] photoactuators,[4,12−14] solar energy conversion,[15,16] photoswitchable devices,[17,18] and bistable photomodulation.[19] The ability to craft micro- and nanostructures of LCP is of pivotal importance for these applications. However, it is notable that the implementation of azobenzene-containing LCPs for a broad range of applications noted above often involves the structuring of LCPs by direct laser writing, imprint, lithography, etc., which typically requires a high-cost operation (e.g., laser writing) or a tedious multistep procedure for pattern fabrication (e.g., lithography) and has low throughput.[20] Clearly, a simple and

Received: October 21, 2017
Accepted: January 8, 2018
Published: January 8, 2018

DOI: 10.1021/acsami.7b16001
ACS Appl. Mater. Interfaces 2018, 10, 4961−4970

cost-effective technique that enables a rapid large-scale production of highly ordered azobenzene-containing LCPs patterns is highly desirable.

The evaporative self-assembly from a sessile drop containing nonvolatile solutes (e.g., coffee, nanoparticles, DNA, pigments, quantum dots, and polymers) represents an extremely simple route to a wide variety of intriguing and complex deposit patterns.[21,22] However, irregular dissipative structures (e.g., randomly organized convection patterns and stochastically distributed multirings) are often yielded due to lack of control over the evaporative flux of solvent and the associated flow within the droplet, the interfacial interaction between solute and substrate, etc.[23,24] Notably, recent advances in harnessing the solvent evaporation process by enforcing confined geometries[25−30] (e.g., curve-on-flat[28,31,32] and wedge-on-flat[33−35] geometries) over a droplet have offered great control of pattern formation, affording access to a rich array of regular structures and assemblies, including gradient concentric "coffee rings",[23,24] hierarchically ordered web,[32] snake-skin-like structures,[31] and two-dimensional grids.[28] As light is a clean, easily accessible, nondestructive, and remotely controllable stimulus, the ability to assemble photoresponsive polymers into well-ordered structures by steering solvent evaporation in confined geometries may entail the speedy creation of desirable photoresponsive patterns.

Herein, we report on a convenient and rapid route to hierarchical azobenzene-containing LCP stripes over a large area via flow-enabled self-assembly (FESA). These hierarchical stripes can be reversibly photoswitched. First, the LCP solution was allowed to dry in a two-nearly-parallel-plate geometry, in which the upper plate was fixed, whereas the lower plate placed on a translational stage was programmably traveled in a "stop-and-move" manner (i.e., a FESA process), yielding photoswitchable LCP stripes that exhibited two forms of periodic LCP deposits. They are large-dimension primary stripes and small-dimension secondary stripes regularly situated between adjacent primary stripes (i.e., forming hierarchical stripes; and an array of nearly centimeter-scale stripes can be produced in less than 3 min). The size (width w_S and height h_S) and the distance between two adjacent secondary stripes (λ_S) were largely dictated by a set of parameters, including the solution concentration (c), the moving speed of the lower plate (v), and the separation distance of two plates (H). Subsequently, the photoresponsive behavior of hierarchical LCP stripes was scrutinized by in situ polarized optical microscopy and UV−vis spectroscopy studies, revealing a nonsynchronized photoisomerization process arising from the thickness difference between primary and secondary stripes (i.e., secondary stripes disappear prior to primary stripes upon UV irradiation; primary stripes recover ahead of secondary stripes upon subsequent visible light exposure). Detailed exploration revealed that the stripes expanded when exposed to UV light and the expansion can be partially restored. In addition to LCP, hierarchical patterns were also produced by one-step FESA using other polymers.

RESULTS AND DISCUSSION

In our study, an LCP poly(6-(4-(4-ethoxyphenylazo) phenoxy)-hexyl methacrylate) (PM_6ABOC_2) (Figure 1a) was employed as nonvolatile solute for crafting photoswitchable hierarchical PM_6ABOC_2 stripes by FESA. PM_6ABOC_2 possesses a fast response to UV irradiation and efficient photoisomerization and has been widely used in photo-

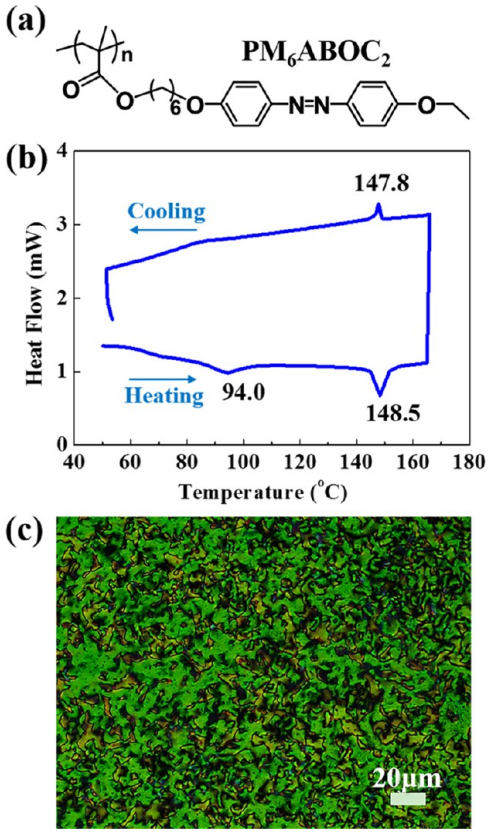

Figure 1. Structure and liquid crystalline property of the liquid crystal polymer (LCP). (a) Chemical structure of poly(6-(4-(4-ethoxyphenylazo)phenoxy)-hexyl methacrylate) (PM_6ABOC_2). (b) Differential scanning calorimetry (DSC) curves of first time cooling and second time heating processes. Upon heating, an LC region ranging from 94 to 148.5 °C is clearly evident. (c) Typical schlieren texture under the polarized optical microscope (POM) at 140 °C.

actuators.[36,37] Scheme S1 shows the synthetic route to PM_6ABOC_2. The success of synthesis was confirmed by ^{1}H NMR (Figure S1). The LC temperature of PM_6ABOC_2 ranges from 94 to 148.5 °C upon heating (Figure 1b). The polarized optical micrograph for the sample annealed at 140 °C displayed a typical schlieren texture, indicating nematic LC phase (Figure 1c).

A drop of PM_6ABOC_2 toluene solution (e.g., concentration, c = 2 mg/mL) at room temperature was loaded in a two-nearly-parallel-plate geometry composed of a stationary upper plate (glass blade) and a moving lower plate (Si substrate for optical microscopy imaging in reflection mode or glass substrate for UV spectroscopy measurement on the photoisomerization process) separated by a certain distance H (Figure 2a). In this study, toluene was chosen to craft well-ordered striped structures over other organic solvents (e.g., tetrahydrofuran (THF) or dimethylformamide (DMF); the obtained patterns using the THF and DMF solutions are shown in Figure S2) due to the following several reasons: toluene is a good solvent for LCP and possesses a proper evaporation rate at room temperature[38] and a proper contact angle with the substrate. In general, the contact angle (θ) between the solution and the substrate is in the range of $0 < \theta < 90°$ to ensure the wetting of the polymer solution.[39,40] Figure S3 showed the contact angle of the LCP toluene solution on different substrates ($\theta_{LCP/Si\ wafer}$ = 4.8° and $\theta_{LCP/glass}$ = 5.2°; no upper plate was applied).

DOI: 10.1021/acsami.7b16001
ACS Appl. Mater. Interfaces 2018, 10, 4961−4970

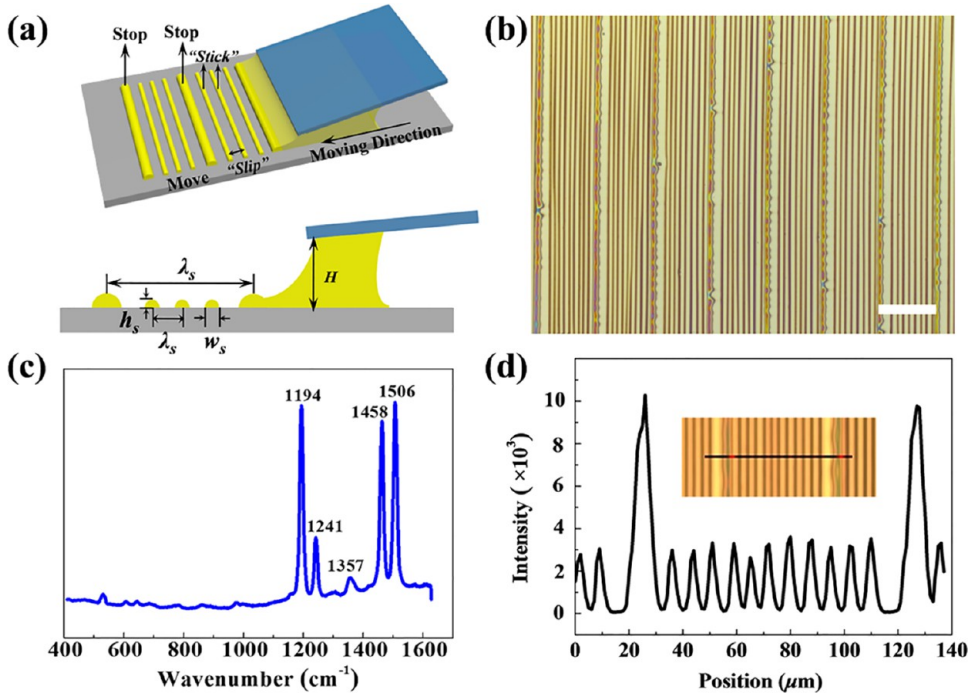

Figure 2. (a) Schematic illustration of the formation of hierarchical stripes composed of photoswitchable PM_6ABOC_2 (upper panel: three-dimensional view; lower panel: side view, where λ_P is the typical distance between two adjacent primary stripes formed via flow-enabled self-assembly (FESA) of a drop of PM_6ABOC_2 toluene solution in a two-nearly-parallel-plate geometry in a stop-and-move mode; λ_S is the characteristic distance between two adjacent secondary stripes yielded by "stick-and-slip" motion of the three-phase contact line during the movement of the lower Si substrate; H is the separation distance between the upper blade and lower Si substrate. w_S and h_S are the width and height of secondary stripes, respectively. (b) A representative optical micrograph of hierarchical stripes over a large area produced via FESA of PM_6ABOC_2 toluene solution at a concentration c of 2 mg/mL and the moving speed of the lower Si substrate of 50 μm/s. Scale bar = 100 μm. (c) The Raman spectrum of PM_6ABOC_2 LCP (laser excitation wavelength: 532 nm; power: 25 mW). The characteristic peaks are as follows: 1458 cm^{-1} for N═N symmetric stretching, 1194 cm^{-1} for C−N symmetric stretching, 1241 cm^{-1} for C−N symmetric bending, and 1506 cm^{-1} for C−C symmetric stretching. (d) The Raman line scanning of hierarchical stripes at the wavenumber of 1458 cm^{-1}, corresponding to the N═N symmetric stretch.

The lower substrate was mounted on a computer-controlled translational stage that enables its stop-and-move mode motion during FESA of PM_6ABOC_2. First, the lower movable Si substrate was stationary for a short period of time t = 1 s (i.e., "stop"), during which the outward flow triggered by the evaporative loss of toluene transported PM_6ABOC_2 to the contact line (a well-known "coffee ring" effect[39]), forming a thick PM_6ABOC_2 stripe (i.e., primary stripe). The Si substrate was then translated (i.e., "move") at a certain moving speed v (e.g., v = 50 μm/s); the meniscus (lower panel in Figure 2a) was stretched and the initial contact angle at the meniscus edge decreased to a critical value, at which the depinning force became larger than the pinning force,[41] leading to the jump of the contact line to new position at which the initial contact angle was resumed (i.e., "slip") and thus forming a new PM_6ABOC_2 stripe (i.e., secondary stripe). The repetitive stick-and-slip cycles of the three-phase contact line yielded a set of periodic secondary stripes until the Si substrate stopped at a new position (i.e., a subsequent stop) (Figure 2a) for the same t = 1 s, where a new primary stripe formed. We define the typical distance between two adjacent primary stripes formed at the stop locations enabled by using the translation stage as λ_P. Accordingly, the characteristic distance between two neighboring secondary stripes at the "stick" locations formed during the movement of the lower Si substrate due to the stick-and-slip motion of the contact line was referred to as λ_S. A representative optical micrograph of hierarchical PM_6ABOC_2 stripes with high regularity formed via FESA by moving the lower Si substrate in a stop-and-move mode mode (forming periodic primary stripes) in conjunction with the stick-and-slip motion of the contact line (forming periodic secondary stripes within two adjacent primary stripes) is shown in Figure 2b. Clearly, the dimension of primary stripes is larger than that of secondary stripes, which was further substantiated by the Raman measurement.[42] As shown in Figure 2c, the most notable peaks of azobenzene-containing PM_6ABOC_2 appeared at 1194 cm^{-1} (C−N symmetric stretch), 1241 cm^{-1} (C−N symmetric bending), 1458 cm^{-1} (N═N symmetric stretch), and 1506 cm^{-1} (C−C symmetric stretch).[43−45] Thus, the N═N symmetric stretch at 1458 cm^{-1} was chosen as a characteristic peak of PM_6ABOC_2 for the Raman line scanning. Figure 2d displays the Raman line scanning at 1458 cm^{-1} over a distance of 140 μm (the corresponding optical micrograph is shown as an inset), clearly revealing a well-defined hierarchical structure composed of 2 higher and wider primary stripes with λ_P of 100 μm and 11 uniformly arranged lower and narrower secondary stripes with λ_S of ∼100/12 = 8.3 μm. Two primary stripes exhibited a much stronger Raman signal, demonstrating the obvious height difference between primary and secondary stripes. Furthermore, the comparison of the intense Raman signal on the stripes and zero counts over the region between secondary stripes confirmed that there was no PM_6ABOC_2 deposited between secondary stripes.[46]

Notably, hierarchical stripes over a large area can be readily and rapidly created simply by one-step FESA (Movie SI). An array of nearly centimeter-scale stripes can be produced in less

DOI: 10.1021/acsami.7b16001
ACS Appl. Mater. Interfaces 2018, 10, 4961−4970

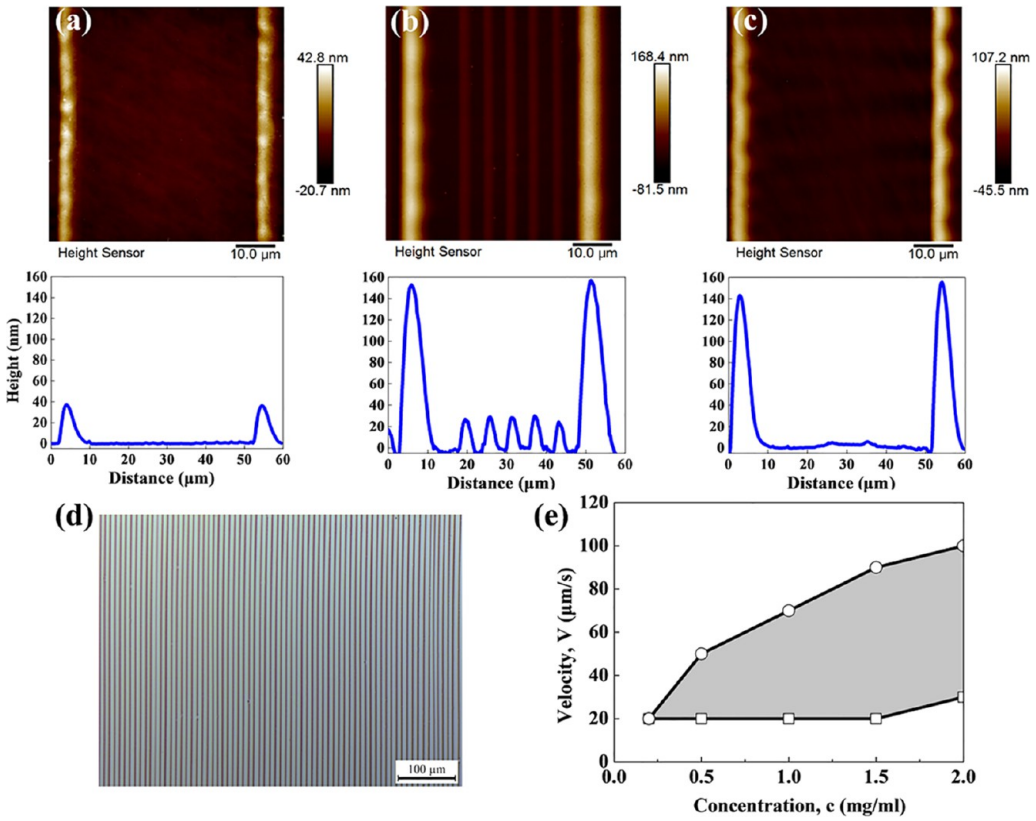

Figure 3. Effect of the solution concentration c and the moving speed of the lower Si substrate v on the formation of hierarchical stripes (λ_P = 50 μm). (a) c = 0.5 mg/mL and v = 50 μm/s, no secondary stripes were formed between primary stripes, (b) c = 2 mg/mL and v = 50 μm/s, secondary stripes were deposited between two primary stripes, and (c) c = 2 mg/mL and v = 100 μm/s, no secondary stripes were produced between primary stripes. (d) Secondary stripes yielded by continuously moving lower Si substrate in a FESA process (i.e., without stop of the lower Si substrate, that is, no formation of primary stripes). The moving speed of the lower Si substrate v is 40 μm/s, the solution concentration c is 2 mg/mL, and the separation distance between the upper glass blade and lower Si substrate H is 100 μm. (e) Two-dimensional (2D) map showing the effect of the moving speed v and the concentration c of azobenzene-containing LCP PM_6ABOC_2 on the formation of secondary stripes. The shadow area indicates the parameters under which periodic secondary stripes form. Outside the shadow area, secondary stripes either disappeared above the upper critical moving speed or connected to each other, forming irregular polymer film below the lower critical moving speed of lower Si substrate.

than 3 min. The drying 6 μL PM_6ABOC_2 toluene solution yielded hierarchical stripes over a surface area of 0.8 × 0.8 cm^2, which is governed by the size of upper stationary glass blade used in the FESA process (0.8 × 0.8 cm^2 in this study) as well as the volume of the PM_6ABOC_2 toluene solution. Obviously, by employing a larger-sized upper plate and continuously supplying the FESA apparatus with solution, hierarchical stripes deposited over an even larger surface area can be conveniently achieved.

It is noteworthy that λ_P and the size of primary stripes (i.e., width w_P and height h_P) can be easily tailored by altering the distance that the lower Si substrate travels and the time the Si substrate stops. Unless otherwise specified, in our study, λ_P of 50 and 100 μm was deliberately obtained for AFM imaging and other characterizations (e.g., optical microscopy imaging, etc.), respectively, and the time for the lower Si substrate to stop was set as 1 s. The undulation along the primary stripe was seen, which may be due to the unfavorable interaction between PM_6ABOC_2 and the Si substrate.[24,47]

As primary stripes were yielded simply by modulating the distance that the lower Si substrate traveled and the stop time it experienced, the creation of primary stripes is straightforward and easily controlled. Thus, we turn our attention to explore the influence of experimental conditions, including the solution concentration (c) and the moving speed of the lower substrate (v) on the formation of secondary stripes. Figure 3 compares AFM height images of three samples obtained via FESA of PM_6ABOC_2 toluene solution at different c and v, while keeping other parameters fixed (i.e., λ_P = 50 μm and the separation distance between upper and lower plates H = 400 μm). At low c (c = 0.5 mg/mL), no secondary stripes were observed when performing FESA of PM_6ABOC_2 toluene solution at v = 50 μm/s (Figure 3a). Clearly, the experimental condition where c = 2 mg/mL and v = 50 μm/s rendered the crafting of an array of periodic secondary stripes. On the other hand, FESA of PM_6ABOC_2 toluene solution (c = 2 mg/mL) at higher v of 100 μm/s also failed to yield secondary stripes. Interestingly, the formation of secondary stripes was found to be independent of the existence of primary stripes, that is, secondary stripes can still be produced at proper moving velocity v and solution concentration c (Figure 3d) by continuously moving the lower Si substrate mounted on the translational stage (i.e., without stop of the Si substrate, namely, with no primary stripes formed).

A further scrutiny of the c and v spaces revealed that the formation of periodic secondary stripes depended heavily on c and v. Figure 3e shows the parameters within the shadow area resulted in the regular secondary stripe arrays. Notably, a minimal critical concentration $c_{critical,min}$ of 0.2 mg/mL that hierarchical stripes can form existed. Below $c_{critical,min}$, no

DOI: 10.1021/acsami.7b16001
ACS Appl. Mater. Interfaces 2018, 10, 4961−4970

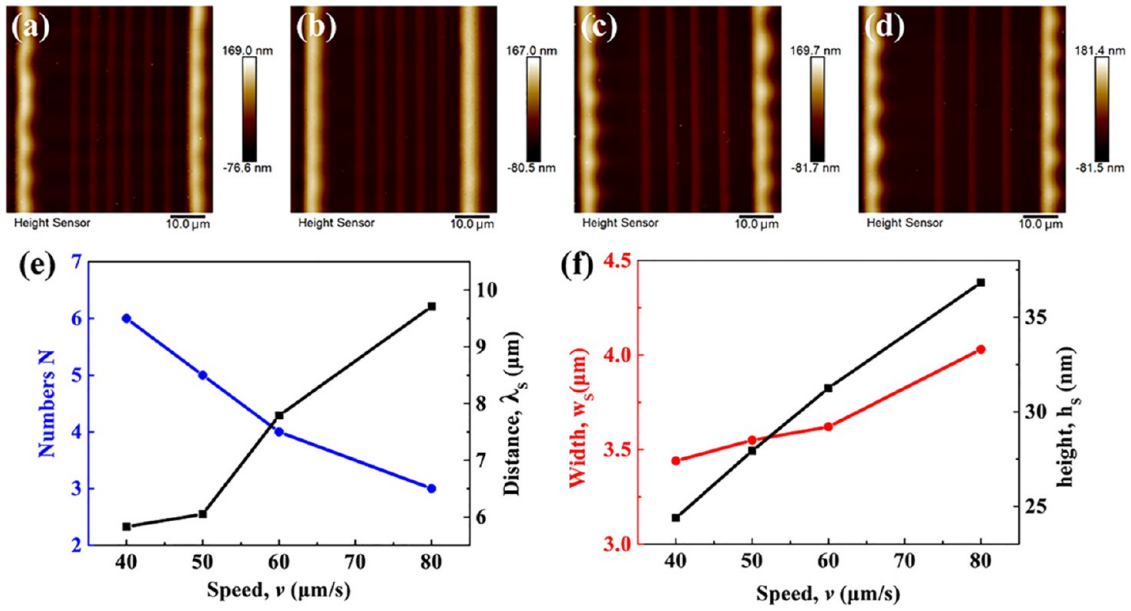

Figure 4. (a–d) AFM images of hierarchical stripes formed by FESA of PM_6ABOC_2 toluene solution (c = 2 mg/mL) at different moving speeds of the lower Si substrate mounted on a translational stage v. (a) v = 40 μm/s, (b) v = 50 μm/s, (c) v = 60 μm/s, and (d) v = 80 μm/s. (e) Influence of moving speed on the number of secondary stripes (N) within two primary stripes (λ_P = 50 μm) and characteristic distance between two adjacent secondary stripes (λ_S). As the moving speed v increased from 40–50 to 60–80 μm/s, N decreased from 6–5 to 4–3, λ_S increased from 5.83–6.05 to 7.79–9.71 μm. (f) The lateral dimension change of each secondary stripe when altering the moving speed of the lower Si substrate. Both width w_S increased from 3.44–3.55 to 3.62–4.03 μm and height h_S increased from 24–28 to 31–37 nm, as the moving speed of the lower Si substrate increased.

secondary stripes were observed, as there was not enough polymers to be pinned at the contact line to form stripes. In the area above the shadow, where v is faster and c is lower, secondary stripes also failed to be produced. Below the shadow area, where v is slower and c is higher, relatively irregular patterns were predominant. From this 2D c–v map, the critical moving speed (i.e., v_{max} and v_{min}) at a certain concentration and the critical concentration (i.e., $c_{critical}$) at a fixed moving speed can also be identified in the shadow area (e.g., at a certain c = 2 mg/mL, critical speeds for forming periodic secondary stripe arrays were v_{max} = 100 μm/s and v_{min} = 30 μm/s, respectively).[48] A slower moving speed enabled sufficient pinning time yet shorter characteristic distance between two adjacent secondary stripes λ_S. For example, at v = 100 μm/s, only 0.5 s was needed for the lower substrate to move from one primary stripe deposit position to the next location (i.e., traveling a distance of 50 μm). However, when v was reduced to 10 μm/s, it took 5 s to reach the next stop position at the same traveling distance of 50 μm, which afforded much longer time for the polymer to undergo stick-and-slip cycles (i.e., pinning and depinning cycles) within two primary stripes, thus leading to the formation of more densely populated secondary arrays, that is, a shortened λ_S.

It has been reported that a critical moving distance (and thus a minimum spacing between two adjacent stripes λ_{min}) is required for the contact line pinning and depinning process to yield a highly ordered pattern.[25] In this study, when λ_S was shorter than $\lambda_{S,min}$ (i.e., $\lambda_S < \lambda_{S,min}$), a relatively irregular pattern formed. Once the moving speed of the lower Si substrate was slow enough (e.g., v = 10 μm/s for 2 mg/mL solution) to induce a smaller λ_S than $\lambda_{S,min}$, secondary stripes became relatively irregular. For the 2 mg/mL solution, as v increased from 40 to 80 μm/s, the number of secondary stripes N within a 50 μm distance defined by two adjacent primary stripes decreased from six to three and λ_S increased from 5.84 to 9.71 μm (Figure 4e). At the same time, both w_S and h_S of secondary stripes increased as a result of the decreased N (Figure 4f). w_S increased from 3.44 to 4.03 μm, and h_S increased from 25 to 37 nm. Compared with higher concentration, at certain moving speed of the lower Si substrate, less PM_6ABOC_2 was deposited to create local surface roughness to pin the contact line at lower concentration. Therefore, secondary stripes were thinner. As c increased from 1 to 2 mg/mL, N decreased from seven to four and λ_S increased from 5.66 to 7.70 μm (Figure S4e); meanwhile, w_S increased from 3.20 to 4.38 μm and h_S increased from 19 to 40 nm (Figure S4f).

It is worth noting that λ_S, w_S, and h_S of secondary stripes can also be tuned by adjusting the separation distance H between the upper glass blade and the lower Si substrate (Figure S5).[28] At the same c and v (i.e., c = 2 mg/mL and v = 50 μm/s), a smaller H entailed more yet thinner secondary stripes. As H decreased from 1000 to 100 μm, N increased from three to six, λ_S decreased from 10.35 to 4.94 μm, and w_S and h_S decreased from 3.68 to 2.82 μm and from 50 to 25 nm, respectively. A decreased H slowed down the evaporation rate of solvent, thus leading to a reduction in the meniscus moving speed.[23,49] Consequently, the contact line recessed over a shorter distance before the formation of a new stripe, resulting in a higher deposition density of secondary stripes. In other words, the reduced evaporative loss of toluene caused the solutes to be deposited less at contact line (i.e., smaller h_S and w_S) and jumped less to the next position where it was pinned again (i.e., shorter λ_S).

As noted above, azobenzene-containing LCPs undergo photoinduced microscopic phase transition due to molecular-level photoisomerization between cis- and trans- conformations upon exposure to light. Compared to other external stimuli, light can be rapidly employed and delivered remotely and

DOI: 10.1021/acsami.7b16001
ACS Appl. Mater. Interfaces 2018, 10, 4961–4970

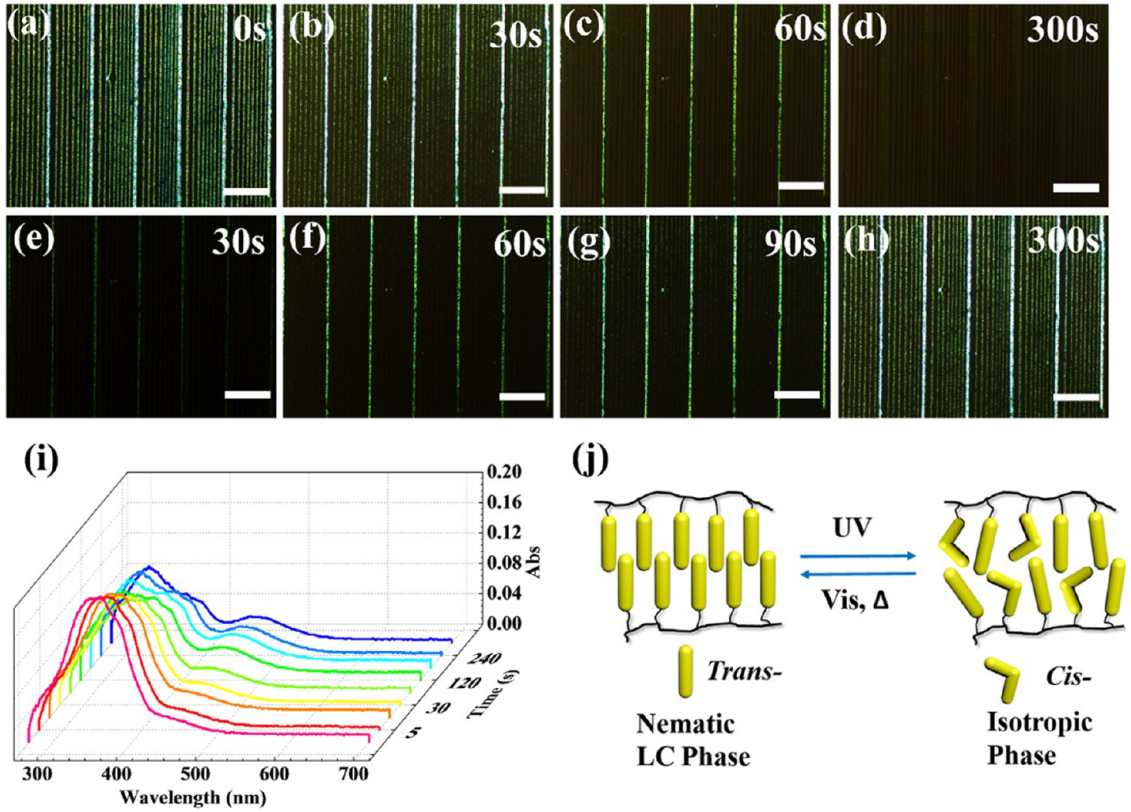

Figure 5. Photoinduced microscopic phase transition of hierarchical stripes composed of azobenzene moieties-containing PM_6ABOC_2 at room temperature. The hierarchical stripes were obtained by FESA of 2 mg/mL PM_6ABOC_2 toluene solution at a moving speed of the lower substrate v = 50 μm/s. (a)−(d) Polarized optical micrographs of hierarchical stripes formed on the Si substrate as UV irradiation time increased: (a) 0 s, (b) 30 s, (c) 60 s, and (d) 300 s. (e)−(h) Polarized optical micrographs of hierarchical stripes recovery as the subsequent visible light irradiation time increased: (e) 30 s, (f) 60 s, (g) 90 s, and (h) 300 s. Scale bar = 100 μm. (i) UV−vis spectra of hierarchical stripes formed on the glass substrate after different UV irradiation times (front to back: 0 s (red), 5, 10, 30, 60, 120, 180, 240, and 300 s (blue)). (j) Schematic illustration of the mechanism of photoinduced phase transition behavior. Left: LC mesogens are in trans- state and the polymer is in nematic LC phase prior to UV irradiation. Right: azobenzenes turn into cis- state, and polymer changes to isotropic phase after UV light irradiation. This process is completely reversible.

instantaneously to the targeted location in a noninvasive manner. In this context, the photoresponsive behavior of crafted hierarchical stripes composed of azobenzene moieties-containing PM_6ABOC_2 was explored. The PM_6ABOC_2 stripes prepared from c = 2 mg/mL and v = 50 μm/s condition were first annealed at 140 °C in a vacuum oven for 12 h to obtain alignment of LC mesogens and then cooled down to room temperature to retain their nematic LC phase.[50,51] After annealing, the LC texture was clearly observed under a polarized optical microscope (Figure 5a). Upon rotation by 45 and 90° under POM, no obvious brightness change was observed (Figure S6), indicating the multidomain nematic phase, that is, the mesogens are not oriented in a certain direction. As trans- mesogens are rodlike and can be maintained in nematic LC phase, whereas bent cis- mesogens destroy the ordered LC phase,[9] an isothermal nematic-to-isotropic phase transition was thus induced upon UV irradiation (Figure 5j). As UV irradiation at room temperature continued, LC textures gradually disappeared owing to the photoinduced nematic-to-isotropic phase transition (Figure 5b−d). An in situ polarized optical microscope observation demonstrated that secondary stripes disappeared first, followed by the extinction of primary stripes. Within a 30 s UV irradiation, secondary stripes vanished first due to lower h_S, whereas primary stripes can still be seen (Figure 5b). A further UV exposure for 300 s resulted in the transition of thicker nematic primary stripes into their isotropic phase. This can be easily understood due to the height difference between primary and secondary stripes. Subsequently, hierarchical stripes in nematic phase were recovered upon visible light irradiation. After a 300 s visible light irradiation, primary and secondary stripes nearly completely reappeared (Figure 5e−h), which can be attributed to the cis-to-trans transition under visible light irradiation (Figure 5j), demonstrating a photoswitching characteristic of hierarchical PM_6ABOC_2 stripes.

In addition to hierarchical stripes formed on the Si substrate, the molecular-level trans−cis photoisomerization behavior was further monitored by UV−vis spectroscopy on samples after being exposed to UV irradiation for different times. These samples were prepared on a transparent glass substrate by FESA of the PM_6ABOC_2 toluene solution. A series of UV−vis absorption curves obtained after exposing to UV for different times (0, 5, 10, 30, 60, 120, 180, 240, and 300 s) are shown in Figure 5i. The absorption peak of trans- mesogens at 358 nm represents a $\pi-\pi^*$ excitation of the azobenzene group, whereas the absorption peak of cis- isomers at 452 nm indicates a $n-\pi^*$ transition.[52−54] Prior to exposure to UV light, the $\pi-\pi^*$ excitation peak at 358 nm was prominent and the $n-\pi^*$ transition peak at 452 nm was almost invisible, signifying a trans- rich state. As the UV irradiation time progressed, the $\pi-\pi^*$ peak at 358 nm dropped and gradually shifted to 317 nm. In the meantime, the $n-\pi^*$ transition at 452 nm emerged and

DOI: 10.1021/acsami.7b16001
ACS Appl. Mater. Interfaces 2018, 10, 4961−4970

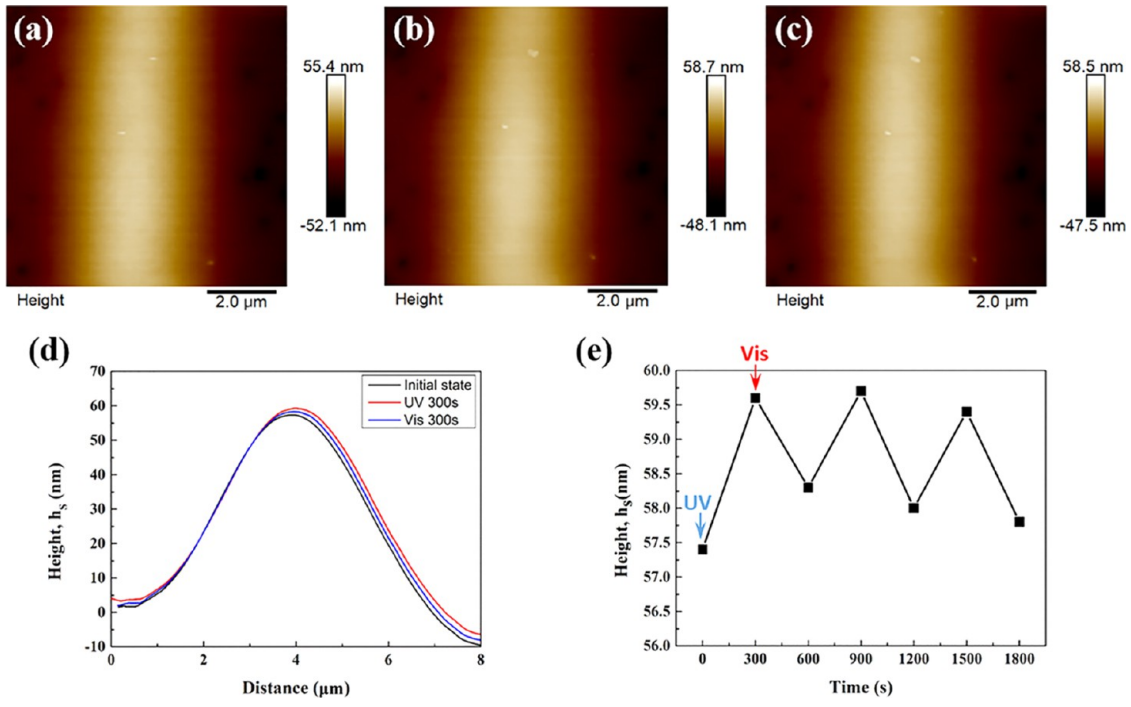

Figure 6. Photoinduced height change and reversibility of a secondary stripe. (a)−(c) AFM images of the stripe: (a) initial state before UV irradiation. (b) UV irradiation for 300 s. (c) Visible light irradiation for 300 s. (d) Height profiles of (a)−(c), respectively. Black curve, initial height of (a), h_S = 57.3 nm; red curve, UV irradiated height of (b), h_S = 59.6 nm; blue curve, visible light recovery of (c), h_S = 58.3 nm. (e) Reversibility of h_S after repeated UV−vis irradiation cycles.

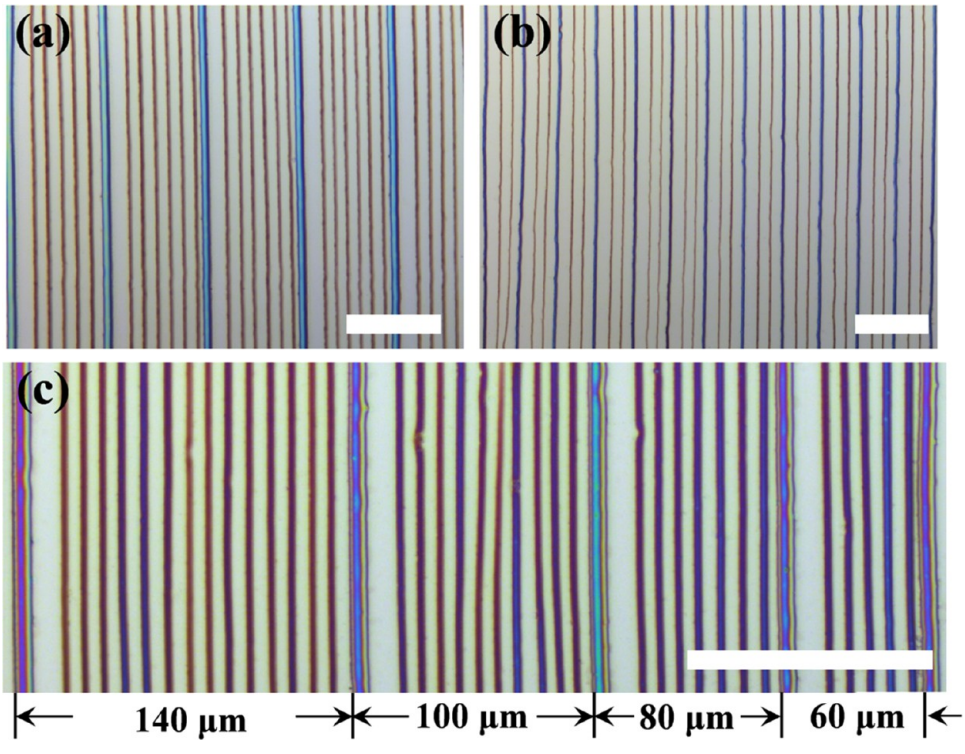

Figure 7. Hierarchical stripes and gradient hierarchical stripes obtained by FESA of PS or PMMA toluene solution. (a) Hierarchical stripes composed of PS (molecular weight, M_w = 420 K; characteristic distance between two adjacent secondary stripes λ_P = 100 μm; solution concentration c = 0.5 mg/mL; moving speed of lower Si substrate v = 50 μm/s; stop time of lower Si substrate t = 1 s). (b) Hierarchical stripes composed of PMMA (M_w = 800 K, λ_P = 50 μm, c = 0.5 mg/mL, v = 30 μm/s, and t = 0.5 s). (c) Gradient hierarchical stripes composed of PS (M_w = 420 K, λ_P = 140, 100, 80, and 60 μm from left to right; c = 1 mg/mL; v = 40 μm/s; and t = 1 s). Scale bar = 100 μm.

gradually increased, suggesting the transition from trans-mesogens to cis- isomers.

The height of a certain secondary stripe (h_S) before UV light irradiation as well as with UV (365 nm, 100 mw/cm^2)

DOI: 10.1021/acsami.7b16001
ACS Appl. Mater. Interfaces 2018, 10, 4961−4970

irradiation for 300 s followed by visible light irradiation (460 nm, 100 mw/cm^2) for 300 s (Figure 6a−c) was measured. The initial height of a secondary stripe is 57.3 nm, the UV light irradiation induced the height photoexpansion to 59.6 nm, representing a 4% expansion. The subsequent visible light irradiation can only partially recover the height to 58.3 nm (a 1.7% expansion compared to that of the initial height; Figure 6d). The repeated UV−vis light irradiation cycles resulted in a reversible expansion upon the UV light exposure and a recovery with the visible light exposure (Figure 6e). We note that the similar phenomenon has been reported in the literature.[55] The photoexpansion effect can be attributed to the requirement of more free volume due to the trans−cis conformational change. The first-time expansion is composed of the volume expansion of cis- chromophore compared with that of trans- and the expansion of the polymer matrix. The trans−cis−trans conformational change contributed to the reversible expansion, whereas the increase of free volume trapped in the polymer matrix cannot be fully recovered to the initial height owing to the high T_g of LCP (95 °C) at room temperature.

Interestingly, the FESA strategy is viable and robust; in addition to hierarchical stripes produced using LCP, hierarchical stripes of other polymers can also be conveniently crafted. Figure 7a,b shows hierarchical stripes of polystyrene (PS) and poly(methyl methacrylate) (PMMA) formed in the same manner as PM_6ABOC_2. More intriguingly, by judiciously manipulating the typical distance of primary stripes λ_P, a gradient hierarchical structure can also be achieved (Figure 7c). As λ_P decreased from 140−100 to 80−60 μm, the number of secondary stripes within two primary stripes changed accordingly from 14−10 to 7−5 (Figure 7c). Such a gradient hierarchical pattern may find potential applications in encoding and cell motility study.

CONCLUSIONS

In summary, hierarchical photoswitchable stripes consisting of smaller-sized secondary stripes situated between larger-sized primary stripes were, for the first time, exquisitely crafted over large areas by flow-enabled self-assembly of azobenzene-containing LCP in a two-nearly-parallel-plate geometry that renders the control over solvent evaporation. The primary and secondary stripes were yielded as a direct consequence of repetitive stop-and-move mode motion of the lower substrate in the two-nearly-parallel-plate geometry and stick-and-slip cycle of the contact line, respectively. The moving speed of the lower substrate and solution concentration exerted a profound influence on the formation of secondary stripes. A relatively slow moving speed and higher solution concentration favored the creation of periodic secondary stripes. The separation distance between the upper blade and lower substrate also impacted the dimension of secondary stripes. The hierarchical stripes displayed a microscopic reversible photoinduced LC-to-isotropic phase transition due to the molecular-level trans-to-cis photoisomerization of azobenzene moieties. A UV light-induced photoexpansion effect was observed on the LCP stripes, which can be partially recovered after visible light irradiation. The height difference between primary and secondary stripes conferred the phase transition of these hierarchical stripes to occur sequentially, which may be useful for photoswitchable materials and devices. Furthermore, hierarchical stripes were also achieved in other polymers such as PS and PMMA. A gradient hierarchical PS stripe was also constructed. As such, FESA may provide a convenient and robust means to arrange a wide range of building blocks, including polymers, colloids, nanocrystals, graphene, etc., into complex patterns over a large area with exquisite control over the periodicity. They may find application in solar cells as the light trapping layer to improve light-harvesting efficiency,[56] tribolelectric nanogenerators by increasing the effective contact area and thus the output voltage and current,[57] cell motility and adhesion, and cell mechanotransduction.[58,59]

EXPERIMENTAL SECTION

Synthesis of Liquid Crystalline Polymer Poly(6-(4-(4-ethoxyphenylazo)phenoxy)-hexyl methacrylate) (PM_6ABOC_2). *Synthesis of Monomer M_6ABOC_2.* The monomer M_6ABOC_2 was prepared by a three-step procedure according to the literature.[50] First, 4-ethoxy-4′-hydroxyazobenzene (compound 1 in Scheme S1) was obtained via a diazo coupling reaction between 4-ethoxyaniline and phenol in the presence of sodium nitrite and hydrochloric acid. Second, the 4-ethoxy-4′-hydroxyazobenzene (compound 2 in Scheme S1) was mixed together with 6-chloro-1-hexanol, potassium carbonate, and a trace amount of potassium iodide in ethanol and then refluxed for 12 h to produce 4-ethoxy-4-(6-hydroxy hexyloxy). Finally, the monomer M_6ABOC_2 was produced by the esterification reaction between 4-ethoxy-4-(6-hydroxy hexyloxy) and methacryloyl. The monomer was purified by recrystallization in methanol.

Synthesis of PM_6ABOC_2. Liquid crystal polymer poly(6-(4-(4-ethoxyphenylazo)phenoxy)-hexyl methacrylate) (PM_6ABOC_2) was synthesized by free radical polymerization of M_6ABOC_2 using 2,2-azobisisobutyronitrile (AIBN) as initiators at 70 °C in anhydrous DMF and was then purified by precipitation in methanol three times. The molecular weight of the obtained polymer is M_n = 24k (polydispersity index = 1.61). The ^{1}H NMR spectrum of the purified polymer is shown in Figure S1.

Flow-Enabled Self-Assembly of Photoswitchable PM_6ABOC_2 Solution. A drop of PM_6ABOC_2 toluene solution with concentration varied from 0.2 to 3 mg/mL was loaded in a two-nearly-parallel-plate geometry constructed by placing an upper glass blade over a lower Si substrate with a separation distance between them controlled by a micrometer. The Si substrate was mounted on a translational stage (Parker Hannifin Corp, mode: MX80LVixBL2b), of which the moving speed and stopping time can be controlled by computer. Humidity and temperature were kept the same throughout all experiments.

Photoresponsive Behavior of PM_6ABOC_2 Strips. After the flow-enabled self-assembly process, PM_6ABOC_2 stripes were annealed at 140 °C for 12 h in vacuum and cooled down to room temperature to keep their LC phase. The resulting stripes with LC texture were observed under a polarized optical microscope (POM). Visible light photoirradiation process was performed with a 100 W mercury lamp, and the UV light was obtained with the same light source using a 365 nm UV filter mounted on an optical microscope. The LC-textured stripes were exposed to 365 nm UV light to observe the phase transition.

Characterizations. The optical image and LC texture of PM_6ABOC_2 stripes were obtained by an optical microscope (Olympus BX51). The AFM image was conducted in tapping mode (Bruker Dimension Icon 3100), and the force constant of the probe is 40 N/m. The Raman measurement were performed using laser, with the excitation wavelength of 532 nm and power of 25 mW (Renishaw, in-Via). The photoisomerization behavior was examined by a Shimadzu UV-2600 spectrometer. A differential scanning calorimetry (DSC8000, PerkinElmer) was used to determine thermal properties of LCP.

ASSOCIATED CONTENT

Supporting Information

The Supporting Information is available free of charge on the ACS Publications website at DOI: 10.1021/acsami.7b16001.

Synthetic process, ^{1}H NMR, DSC curve, POM image, and the Raman spectrum of PM_6ABOC_2 liquid crystalline polymer; influence of the concentration (c)

DOI: 10.1021/acsami.7b16001
ACS Appl. Mater. Interfaces 2018, 10, 4961−4970

and the separation distance between the upper blade and lower substrate (H) on the size of secondary stripes (PDF)

Movie of the formation of hierarchical photoswitchable stripes by FESA (AVI)

AUTHOR INFORMATION

Corresponding Authors

*E-mail: slin@ecust.edu.cn (S.L.).
*E-mail: yuhaifeng@pku.edu.cn (H.Y.).
*E-mail: zhiqun.lin@mse.gatech.edu (Z.L.).

ORCID

Zhonglin Wang: 0000-0002-5530-0380
Shaoliang Lin: 0000-0003-3374-9934
Haifeng Yu: 0000-0003-0398-5055
Zhiqun Lin: 0000-0003-3158-9340

Notes

The authors declare no competing financial interest.

ACKNOWLEDGMENTS

This work is supported by the Air Force Office of Scientific Research (FA9550-16-1-0187), the National Science Foundation (CMMI 1562075 and 1727313; DMR 1709420), and National Natural Science Foundation of China (grant nos. 51322301, 51573005, 51622301, and 51573046). This research was also supported by the BK21 Plus program through the National Research Foundation of Korea funded by the Ministry of Education. X.L. gratefully acknowledges the financial support from the China Scholarship Council.

REFERENCES

(1) Weis, P.; Wang, D.; Wu, S. Visible-Light-Responsive Azopolymers with Inhibited π-π Stacking Enable Fully Reversible Photopatterning. *Macromolecules* **2016**, *49*, 6368−6373.
(2) Ware, T. H.; McConney, M. E.; Wie, J. J.; Tondiglia, V. P.; White, T. J. Voxelated liquid crystal elastomers. *Science* **2015**, *347*, 982−984.
(3) Lv, J. A.; Liu, Y.; Wei, J.; Chen, E.; Qin, L.; Yu, Y. Photocontrol of fluid slugs in liquid crystal polymer microactuators. *Nature* **2016**, *537*, 179−184.
(4) Gelebart, A. H.; Mulder, D. J.; Varga, M.; Konya, A.; Vantomme, G.; Meijer, E.; Selinger, R. L.; Broer, D. J. Making waves in a photoactive polymer film. *Nature* **2017**, *546*, 632−636.
(5) Yu, H. Photoresponsive liquid crystalline block copolymers: from photonics to nanotechnology. *Prog. Polym. Sci.* **2014**, *39*, 781−815.
(6) Yu, H. Recent advances in photoresponsive liquid-crystalline polymers containing azobenzene chromophores. *J. Mater. Chem. C* **2014**, *2*, 3047−3054.
(7) Beharry, A. A.; Sadovski, O.; Woolley, G. A. Azobenzene photoswitching without ultraviolet light. *J. Am. Chem. Soc.* **2011**, *133*, 19684−19687.
(8) Zhang, X.; Zhang, J.; Sun, Y.; Yang, H.; Yu, H. Erasable thin-film optical diode based on a photoresponsive liquid crystal polymer. *Nanoscale* **2014**, *6*, 3854−3860.
(9) Ikeda, T.; Tsutsumi, O. Optical switching and image storage by means of azobenzene liquid-crystal films. *Science* **1995**, *268*, 1873.
(10) Seki, T. Light-directed alignment, surface morphing and related processes: recent trends. *J. Mater. Chem. C* **2016**, *4*, 7895−7910.
(11) Yu, H.; Okano, K.; Shishido, A.; Ikeda, T.; Kamata, K.; Komura, M.; Iyoda, T. Enhancement of Surface-Relief Gratings Recorded on Amphiphilic Liquid-Crystalline Diblock Copolymer by Nanoscale Phase Separation. *Adv. Mater.* **2005**, *17*, 2184−2188.
(12) Cheng, Z.; Wang, T.; Li, X.; Zhang, Y.; Yu, H. NIR-Vis-UV light-responsive actuator films of polymer-dispersed liquid crystal/graphene oxide nanocomposites. *ACS Appl. Mater. Interfaces* **2015**, *7*, 27494−27501.
(13) Yu, L.; Yu, H. Light-powered tumbler movement of graphene oxide/polymer nanocomposites. *ACS Appl. Mater. Interfaces* **2015**, *7*, 3834−3839.
(14) Yu, H.; Ikeda, T. Photocontrollable Liquid-Crystalline Actuators. *Adv. Mater.* **2011**, *23*, 2149−2180.
(15) Kucharski, T. J.; Ferralis, N.; Kolpak, A. M.; Zheng, J. O.; Nocera, D. G.; Grossman, J. C. Templated assembly of photoswitches significantly increases the energy-storage capacity of solar thermal fuels. *Nat. Chem.* **2014**, *6*, 441−447.
(16) Feng, W.; Li, S.; Li, M.; Qin, C.; Feng, Y. An energy-dense and thermal-stable bis-azobenzene/hybrid templated assembly for solar thermal fuel. *J. Mater. Chem. A* **2016**, *4*, 8020−8028.
(17) Baroncini, M.; d'Agostino, S.; Bergamini, G.; Ceroni, P.; Comotti, A.; Sozzani, P.; Bassanetti, I.; Grepioni, F.; Hernandez, T. M.; Silvi, S.; et al. Photoinduced reversible switching of porosity in molecular crystals based on star-shaped azobenzene tetramers. *Nat. Chem.* **2015**, *7*, 634−640.
(18) Zhou, H.; Xue, C.; Weis, P.; Suzuki, Y.; Huang, S.; Koynov, K.; Auernhammer, G. K.; Berger, R.; Butt, H.-J.; Wu, S. Photoswitching of glass transition temperatures of azobenzene-containing polymers induces reversible solid-to-liquid transitions. *Nat. Chem.* **2017**, *9*, 145−151.
(19) Bléger, D.; Schwarz, J.; Brouwer, A. M.; Hecht, S. o-Fluoroazobenzenes as readily synthesized photoswitches offering nearly quantitative two-way isomerization with visible light. *J. Am. Chem. Soc.* **2012**, *134*, 20597−20600.
(20) Wang, W.; Du, C.; Wang, X.; He, X.; Lin, J.; Li, L.; Lin, S. Directional photomanipulation of breath figure arrays. *Angew. Chem., Int. Ed.* **2014**, *53*, 12116−12119.
(21) Han, W.; He, M.; Byun, M.; Li, B.; Lin, Z. Large-scale hierarchically structured conjugated polymer assemblies with enhanced electrical conductivity. *Angew. Chem., Int. Ed.* **2013**, *52*, 2564−8.
(22) Han, W.; Lin, Z. Learning from "Coffee Rings": Ordered Structures Enabled by Controlled Evaporative Self-Assembly. *Angew. Chem., Int. Ed.* **2012**, *51*, 1534−1546.
(23) Xu, J.; Xia, J.; Lin, Z. Evaporation-induced self-assembly of nanoparticles from a sphere-on-flat geometry. *Angew. Chem., Int. Ed.* **2007**, *46*, 1860−3.
(24) Hong, S. W.; Xia, J.; Lin, Z. Spontaneous Formation of Mesoscale Polymer Patterns in an Evaporating Bound Solution. *Adv. Mater.* **2007**, *19*, 1413−1417.
(25) Li, B.; Han, W.; Jiang, B.; Lin, Z. Crafting threads of diblock copolymer micelles via flow-enabled self-assembly. *ACS Nano* **2014**, *8*, 2936−2942.
(26) Kim, H. S.; Lee, C. H.; Sudeep, P.; Emrick, T.; Crosby, A. J. Nanoparticle stripes, grids, and ribbons produced by flow coating. *Adv. Mater.* **2010**, *22*, 4600−4604.
(27) Lee, D. Y.; Pham, J. T.; Lawrence, J.; Lee, C. H.; Parkos, C.; Emrick, T.; Crosby, A. J. Macroscopic nanoparticle ribbons and fabrics. *Adv. Mater.* **2013**, *25*, 1248−1253.
(28) Li, B.; Han, W.; Byun, M.; Zhu, L.; Zou, Q.; Lin, Z. Macroscopic highly aligned DNA nanowires created by controlled evaporative self-assembly. *ACS Nano* **2013**, *7*, 4326−4333.
(29) Li, B.; Zhang, C.; Jiang, B.; Han, W.; Lin, Z. Flow-Enabled Self-Assembly of Large-Scale Aligned Nanowires. *Angew. Chem., Int. Ed.* **2015**, *54*, 4250−4254.
(30) Li, B.; Jiang, B.; Han, W.; He, M.; Li, X.; Wang, W.; Hong, S. W.; Byun, M.; Lin, S.; Lin, Z. Harnessing Colloidal Crack Formation by Flow-Enabled Self-Assembly. *Angew. Chem., Int. Ed.* **2017**, *129*, 4625−4630.
(31) Byun, M.; Laskowski, R. L.; He, M.; Qiu, F.; Jeffries-El, M.; Lin, Z. Controlled evaporative self-assembly of hierarchically structured regioregular conjugated polymers. *Soft Matter* **2009**, *5*, 1583−1586.
(32) Hong, S. W.; Wang, J.; Lin, Z. Evolution of ordered block copolymer serpentines into a macroscopic, hierarchically ordered web. *Angew. Chem., Int. Ed.* **2009**, *48*, 8356−8360.

DOI: 10.1021/acsami.7b16001
ACS Appl. Mater. Interfaces 2018, 10, 4961−4970

(33) Hong, S. W.; Byun, M.; Lin, Z. Robust self-assembly of highly ordered complex structures by controlled evaporation of confined microfluids. *Angew. Chem., Int. Ed.* **2009**, *48*, 512−6.
(34) Byun, M.; Han, W.; Qiu, F.; Bowden, N. B.; Lin, Z. Hierarchically ordered structures enabled by controlled evaporative self-assembly. *Small* **2010**, *6*, 2250−5.
(35) Byun, M.; Han, W.; Li, B.; Xin, X.; Lin, Z. An unconventional route to hierarchically ordered block copolymers on a gradient patterned surface through controlled evaporative self-assembly. *Angew. Chem., Int. Ed.* **2013**, *52*, 1122−7.
(36) Zhao, Y.; Bai, S.; Dumont, D.; Galstian, T. V. Mechanically Tunable Diffraction Gratings Recorded on an Azobenzene Elastomer. *Adv. Mater.* **2002**, *14*, 512−514.
(37) Yu, H.; Kobayashi, T.; Hu, G.-H. Photocontrolled microphase separation in a nematic liquid-crystalline diblock copolymer. *Polymer* **2011**, *52*, 1554−1561.
(38) He, M.; Li, B.; Cui, X.; Jiang, B.; He, Y.; Chen, Y.; O'Neil, D.; Szymanski, P.; Ei-Sayed, M. A.; Huang, J. Meniscus-assisted solution printing of large-grained perovskite films for high-efficiency solar cells. *Nat. Commun.* **2017**, *8*, No. 16045.
(39) Deegan, R. D.; Bakajin, O.; Dupont, T. F.; Huber, G.; Nagel, S. R.; Witten, T. A. Capillary flow as the cause of ring stains from dried liquid drops. *Nature* **1997**, *389*, 827−829.
(40) Semenov, S.; Starov, V.; Rubio, R.; Velarde, M. Instantaneous distribution of fluxes in the course of evaporation of sessile liquid droplets: computer simulations. *Colloids Surf., A* **2010**, *372*, 127−134.
(41) Xu, J.; Xia, J.; Hong, S. W.; Lin, Z.; Qiu, F.; Yang, Y. Self-assembly of gradient concentric rings via solvent evaporation from a capillary bridge. *Phys. Rev. Lett.* **2006**, *96*, No. 066104.
(42) Stuart, C. M.; Frontiera, R. R.; Mathies, R. A. Excited-state structure and dynamics of cis-and trans-azobenzene from resonance Raman intensity analysis. *J. Phys. Chem. A* **2007**, *111*, 12072−12080.
(43) Amer, N. M.; Shen, Y. Raman Scattering from Nematic Liquid-Crystalline Azoxybenzenes. *J. Chem. Phys.* **1972**, *56*, 2654−2664.
(44) Trotter, P. Azo dye tautomeric structures determined by laser-Raman spectroscopy. *Appl. Spectrosc.* **1977**, *31*, 30−35.
(45) Koide, S.; Udagawa, Y.; Mikami, N.; Kaya, K.; Ito, M. The Resonance Raman Effect of Azobenzene and p-Aminoazobenzene. *Bull. Chem. Soc. Jpn.* **1972**, *45*, 3542−3543.
(46) Hong, S. W.; Jeong, W.; Ko, H.; Kessler, M. R.; Tsukruk, V. V.; Lin, Z. Directed Self-Assembly of Gradient Concentric Carbon Nanotube Rings. *Adv. Funct. Mater.* **2008**, *18*, 2114−2122.
(47) Byun, M.; Bowden, N. B.; Lin, Z. Hierarchically organized structures engineered from controlled evaporative self-assembly. *Nano Lett.* **2010**, *10*, 3111−7.
(48) Byun, M.; Hong, S. W.; Zhu, L.; Lin, Z. Self-assembling semicrystalline polymer into highly ordered, microscopic concentric rings by evaporation. *Langmuir* **2008**, *24*, 3525−3531.
(49) Byun, M.; Hong, S. W.; Qiu, F.; Zou, Q.; Lin, Z. Evaporative organization of hierarchically structured polymer blend rings. *Macromolecules* **2008**, *41*, 9312−9317.
(50) Yu, H.; Naka, Y.; Shishido, A.; Ikeda, T. Well-defined liquid-crystalline diblock copolymers with an azobenzene moiety: synthesis, photoinduced alignment and their holographic properties. *Macromolecules* **2008**, *41*, 7959−7966.
(51) Priimagi, A.; Barrett, C. J.; Shishido, A. Recent twists in photoactuation and photoalignment control. *J. Mater. Chem. C* **2014**, *2*, 7155−7162.
(52) Natansohn, A.; Rochon, P. Photoinduced motions in azo-containing polymers. *Chem. Rev.* **2002**, *102*, 4139−4176.
(53) Ikeda, T. Photomodulation of liquid crystal orientations for photonic applications. *J. Mater. Chem.* **2003**, *13*, 2037−2057.
(54) Bisoyi, H. K.; Li, Q. Light-driven liquid crystalline materials: from photo-induced phase transitions and property modulations to applications. *Chem. Rev.* **2016**, *116*, 15089−15166.
(55) Tanchak, O. M.; Barrett, C. J. Light-induced reversible volume changes in thin films of azo polymers: the photomechanical effect. *Macromolecules* **2005**, *38*, 10566−10570.
(56) Na, S. I.; Kim, S. S.; Jo, J.; Oh, S. H.; Kim, J.; Kim, D. Y. Efficient polymer solar cells with surface relief gratings fabricated by simple soft lithography. *Adv. Funct. Mater.* **2008**, *18*, 3956−3963.
(57) Park, J. H.; Park, K. J.; Jiang, T.; Sun, Q.; Huh, J.-H.; Wang, Z. L.; Lee, S.; Cho, J. H. Light-transformable and -healable triboelectric nanogenerators. *Nano Energy* **2017**, *38*, 412−418.
(58) Rianna, C.; Calabuig, A.; Ventre, M.; Cavalli, S.; Pagliarulo, V.; Grilli, S.; Ferraro, P.; Netti, P. A. Reversible holographic patterns on azopolymers for guiding cell adhesion and orientation. *ACS Appl. Mater. Interfaces* **2015**, *7*, 16984−16991.
(59) Rianna, C.; Rossano, L.; Kollarigowda, R. H.; Formiggini, F.; Cavalli, S.; Ventre, M.; Netti, P. A. Spatio-Temporal Control of Dynamic Topographic Patterns on Azopolymers for Cell Culture Applications. *Adv. Funct. Mater.* **2016**, *26*, 7572−7580.

NOTE ADDED AFTER ASAP PUBLICATION

Due to a production error, this paper was published on the Web on January 17, 2018, with a minor misspelling in the title of the paper. The corrected version was reposted on January 23, 2018.

DOI: 10.1021/acsami.7b16001
ACS Appl. Mater. Interfaces 2018, 10, 4961−4970